ELSEVIER

Nuclear Physics B (Proc. Suppl.) 113 (2002) 71–78

NUCLEAR PHYSICS B
PROCEEDINGS
SUPPLEMENTS

www.elsevier.com/locate/npe

The Sileye-3/Alteino experiment on board the International Space Station

M. Casolino[a*], V. Bidoli[a], G. Furano[a], M. Minori[a], A. Morselli[a], L. Narici[a], P. Picozza[a], E. Reali[a], R. Sparvoli[a], C. Fuglesang[b], W. G. Sannita[c], P. Carlson[d], G. Castellini[e], M. Tesi[e], A. Galper[f], M. Korotkov[f], A. Popov[f], N. Vavilov[f], S. Avdeev[g], V. Benghin[h], V. P. Salnitskii[h], O.I.Shevchenko[h], V.P.Petrov[h], K.A. Trukhanov[h], M. Boezio[i], W. Bonvicini[i], A. Vacchi[i], G. Zampa[i], N. Zampa[i], G. Mazzenga[j], M. Ricci[j], P. Spillantini[k]

[a]INFN and University of Roma Tor Vergata

[b]European Astronaut Centre, ESA, Cologne

[c]Neurophysiopathology-DISM,Univ. of Genova, Genova, Italy and Dept. of Psychiatry, SUNY, Stoony Brook, NY, USA

[d]Royal Institute of Technology, Stockholm, Sweden

[e]IROE, CNR, Florence, Italy

[f]Moscow State Engineering Physics Institute, Moscow, Russia

[g]Russian SpaceCorporation "Energia" by name Korolev, Korolev, Moscow region, Russia

[h]Institute for Biomedical Problems, Moscow, Russia.

[i]Dept. of Physics, Univ. and INFN, Trieste, Italy

[j]LNF-INFN, Frascati, Italy

[k]Dept. of Physics, Univ. and INFN, Florence, Italy.

The experiment Sileye-3/Alteino was placed on board the International Space Station on 27 April 2002. The instrument is constituted by a cosmic ray silicon detector and an electroencephalograph. The main scientific aims include the investigation of the Light Flash phenomenon, the study of astronaut brain activity in space when subject to cosmic rays, the measurement of the radiation environment and the nuclear abundances inside the ISS. The instrument cosmic ray detector was active for 130 hours. In addition 6 astronaut Light Flash observation sessions were held, resulting in the observation of this phenomenon on the ISS.

1. INTRODUCTION

Cosmic rays in space are the cause of the radiation dose to which astronauts in space are subject. In space the absorbed and equivalent doses - higher than ground values - depend basically from two parameters: 1. from the cosmic ray flux, function of heliospheric phenomena such as the solar cycle (modulation of galactic cosmic rays) and Solar Particle Events. 2. From the construction (hull shielding) and orbit of the spacecraft. Human activity in space has been limited to work in low earth orbit (LEO), at an height of 300-400 km, with the Space Shuttle and for longer periods on Mir Space Station. With reentry of Mir on 23/3/2001 long term permanence in space has moved on the International Space Station (ISS). Up to now the only human missions outside the

*Corresponding Author, casolino@roma2.infn.it, Dept. of Physics, Univ. of Roma Tor Vergata, Via della ricerca scientifica 1, 00133 Roma, Italy.

0920-5632/02/$ – see front matter
PII S0920-5632(02)01824-8

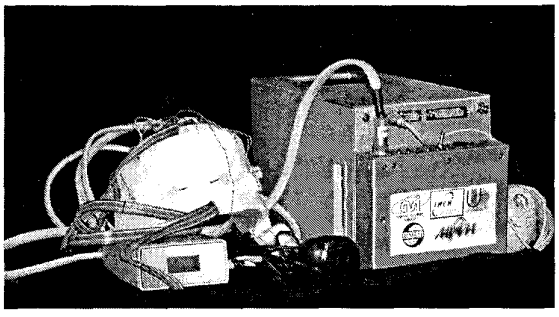

Figure 1. Photo of the Sileye-3/Alteino experiment. On the left is shown the Electroencephalograph, on the right the cosmic ray detector. The joystick to record LF perception is on the extreme right.

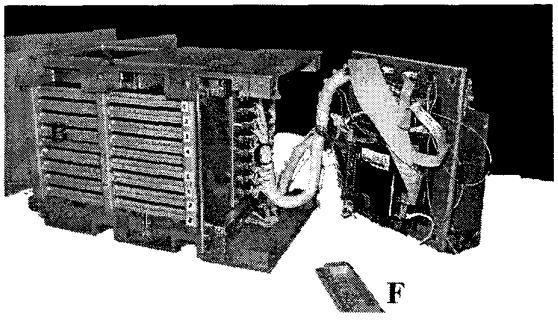

Figure 2. Photo of the cosmic ray detector without the Al protective cover. A: Top (S1) scintillator window. B: Silicon detector frames. C: Read out electronics harness. D: PC-104 CPU above the DSP board. E: Power supply board. F: PCMCIA cover.

protective shielding of the magnetosphere date back to the Apollo program, although long term plans for a future human mission to Mars are under way. Cosmic ray flux and composition is the subject of extensive studies for their importance in different fields of physics, ranging from the cosmological implications of the antimatter component of cosmic rays to solar physics and solar-terrestrial phenomena[1]. Particle energy extends over many orders of magnitude, from the keV range of solar wind to the highest energy ($10^{21} eV$) particles. Cosmic rays of galactic and solar origin are mostly protons and electrons (in equal parts) at the solar wind ($\simeq keV$) energies, with the proton component dominating ($> 90\%$) from the MeV energy range.

All heavier nuclei are present in cosmic rays, with Helium as the most abundant component ($\simeq$ 10%) after Hydrogen ($\simeq 90\%$). In LEO particles can be roughly divided - according to their nature - into galactic, solar and trapped components; their relative abundance and energy spectrum is further complicated by the interposition of the passive material of the hull and the instruments of the spacecraft or the station. For the determination of the equivalent dose absorbed by astronauts is of crucial importance to have a picture of the time and orbit dependent particle rate and composition. A number of detectors have been flying on board spacecraft (Mir[2–4], Shuttle[5–7], ISS[8,9]) to have a detailed picture of the particle fluence in space. In addition to the relatively well quantified absorbed dose, another effect due to the interaction of cosmic rays with the human body is the so called "Light Flash" (LF) phenomenon. Light Flashes are visual phenomena originated by the interaction of cosmic radiation with the human visual apparatus. They are perceived in a variety of shapes (streaks, lines, etc.) and have a different structure from the diffuse glow observed when subject to X rays. This phenomenon was originally predicted by Tobias[10] in 1952 and observed for the first time on board Apollo 11. In the '70s a number of investigations on board Apollo[11,12], Skylab[13], and Apollo-Soyuz Test Project[14] (ASTP) were performed, giving evidence to several mechanisms (direct ionization, Cherenkov light, knock-on protons) without, however, identifying the precise cause and mechanisms involved in this phenomenon. In parallel, a number of ground experiments was also performed using low intensity particle beams on human subjects[15–21,23,24]. The use of a Nitrogen beam, which scanned different regions of the eye[25], seemed to pinpoint the LF phenomenon to occur in the posterior globe of the eye and be in favor of a direct ionization of the retina, although

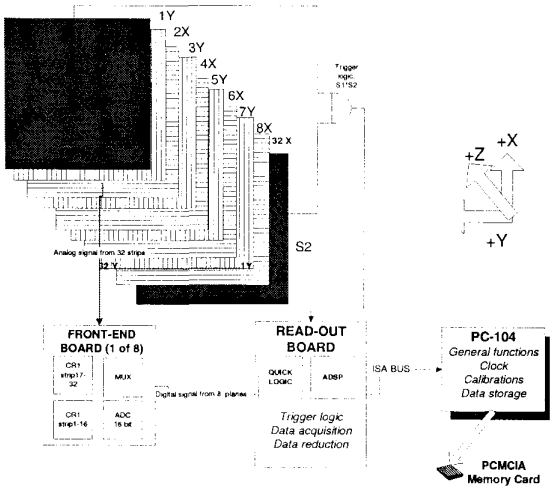

Figure 3. Scheme of the cosmic ray detector: the 8 silicon planes are triggered by two scintillators (S1*S2), converted on the front end boards, read by the Read/out board and saved by the PC-104 on a PCMCIA board.

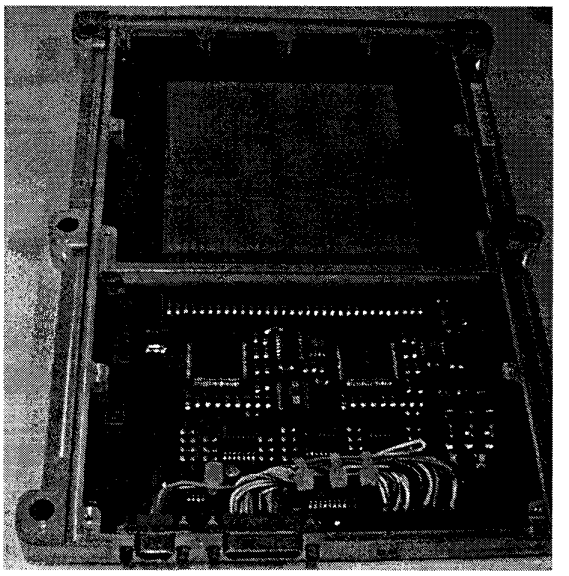

Figure 4. Photo of one of the 8 detector planes (X view). On the upper part top is possible to see the 32 strip segmented silicon wafer. In the lower part is present the preamplifier, analog-to-digital and multiplexing chain. The two connector are for power (left) and signals (right).

LF observed in space may be due to several of the aforementioned effects and be dependent on particle species and energy and therefore on the spacecraft orbit and shielding[22]. The Sileye-3/Alteino experiment is an apparatus devoted to the investigation of the LF phenomenon and the study of cosmic ray particle flux and composition inside the ISS; in addition, astronaut brain activity is monitored with an electroencephalograph (EEG). These three measurements are correlated in real time to provide information on the relationship between cosmic rays and astronauts perception. Sileye-3/Alteino is the third experiment with these aims to fly in a space station: Sileye-1 and -2[26] were operational inside Mir in the years 1995-1998 and 1998-2000 respectively and have provided information on the relative nuclear abundance[27] and LF perception[28].

2. INSTRUMENT DESCRIPTION

As already mentioned, the tasks of Sileye-3/Alteino experiment are manyfold and cover cosmic ray abundance and radiation measurements, brain activity monitoring and investigation of the Light Flash phenomenon. One of the improvements over the first two detectors is the addition of the Electroencephalograph to correlate LF occurrence with measurements of electrophysiology defining the LF time with a greater precision than what could be achieved with the sole pressure of the joystick. To achieve this goal two distinct detectors have been prepared (see Figure 1): the cosmic ray detector (AST - Advanced Silicon Telescope) and the EEG. They can be operated independently, with separate power sources, but are usually used in conjunction to correlate cosmic ray data with LF and EEG measurements. LF perception is recorded on one of the EEG channels with pressure of a joystick button. Additional information is recorded on a dictaphone during LF sessions and on paper after them.

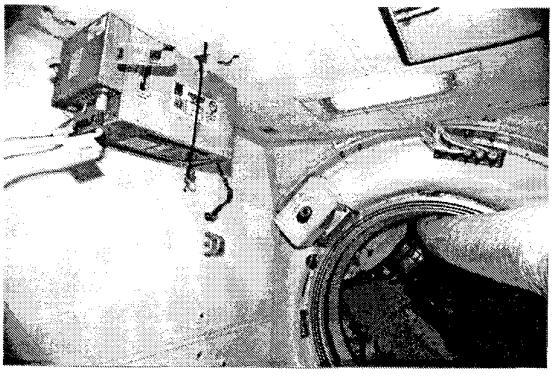

Figure 5. Sileye-3 on its location in the PIRS module on board the International Space Station. The airlock shown in the right part of the picture is connected to the Soyuz-34.

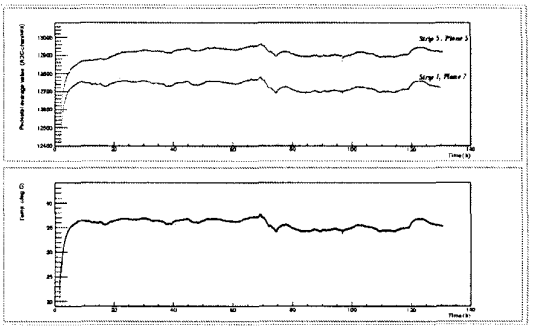

Figure 6. Top Panel: Position of the pedestal of two sample strips of the detector as a function of time. Bottom panel: Temperature inside the detector as a function of time. It is possible to see how the two behaviors are correlated.

2.1. EEG

The electroencephalograph is used to continuously monitor the astronauts brain activity during flight. There are 16 channels, of which one devoted to LF joystick registration, which are sampled with a frequency of 256 Hz and saved on a 64 Mbyte PCMCIA card which is changed each session. The EEG will be described in detail in a separate work.

2.2. Cosmic ray detector - AST

The cosmic ray detector (shown in Figure 2) consists of 8 silicon strip detector planes, each divided in 32 strips, with 2.5 mm pitch. There are 4 planes oriented along the X view and 4 planes along the Y view. The general scheme of the detector is shown in Figure 3. Two scintillators (1 mm thick each) are located on top and bottom of the silicon stack to provide the trigger. The scintillators are covered by a $50\mu m$ Mylar foil located at 12.5 mm from the scintillator, and an Al (70 μm) and Mylar ($50\mu m$) foil at distance 12.5 mm from the mylar plane. In Figure 4 is shown the silicon detector board and the front end electronics, originally developed for the Silicon-Tungsten calorimeter of the magnetic spectrometer PAMELA[29], a satellite-borne apparatus for the study of antimatter component of cosmic rays. Each Silicon plane has a size of 8 cm * 8 cm, with a thickness of $380\mu m$; interplanar distance is 1.4 cm, resulting in a geometric factor of 44.1 cm^2sr. The front-end electronics is based on a VLSI ASIC, the CR1.4P chip[30]. This chip has a dynamic range of 1400 minimum ionizing particle (MIP, 1 MIP= 330 $keV/\mu m \simeq 5.1\ fC$ for $380\mu m$ thick detectors), with good noise performance ($\simeq$ 2700 e^- rms + 5 e^-/pF and low power consumption ($< 100mW/chip$). Each circuit has 16 channels, composed of a charge sensitive preamplifier, a shaping amplifier, a track-and-hold circuit and an output multiplexer. Over the whole range the maximum deviation from linearity is $< 2.5\%$ with an average linearity better than 1%. Outputs are connected to a 16-bit ADC (with serial digital output) through an analogue multiplexer and an operational amplifier. Two CR1 chips are present on each front-end board to read the 32 strips of the silicon plane. A custom Read Out Board performs the tasks of trigger handling and data acquisition. It can be divided in two sections: The Front-end interface logic and the DSP. The Front-end section, based on a Quicklogic fuse programmable logic, includes 8 16-bit shift registers to parallelize serial data coming from ADCs, 3 32-bit counters for the Scintillators (single counters and coincidence signal),

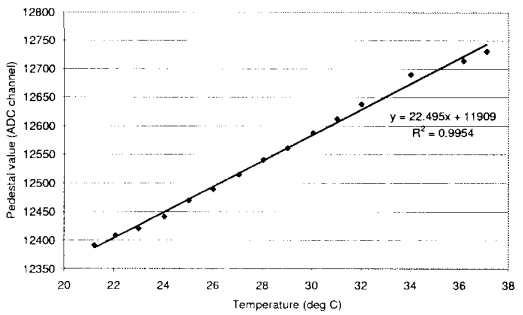

Figure 7. Mean pedestal ADC position as a function of temperature (strip 6).

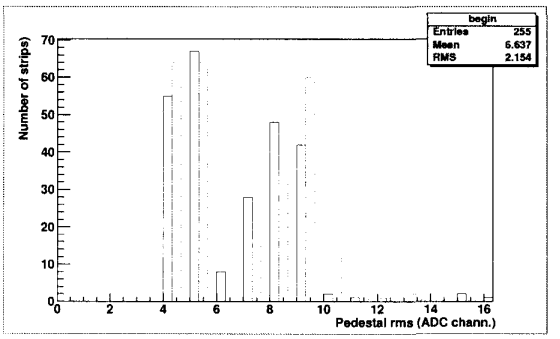

Figure 8. Histogram of the pedestal rms of the detector at the beginning (27/4/02: continuous line) and at the end (2/5/02: dashed line - offset by 0.6 bin for clarity) of the mission.

a programmable delay generator, 16 inputs for temperature alarms with interrupt generator and a 16-bit parallel bus for communication with the DSP. The DSP section is based on the ADSP-2181, a 16-bit integer processor, used for pedestal subtraction and data compression.

The trigger is defined with the logical AND of the signals of the two scintillators $S1$ and $S2$. The trigger gives the hold signal to the preamplifiers (peaked at $1\mu s$) and begins the multiplexed acquisition of the 256 channels and their analog to digital conversion. The DSP then performs data reduction, consisting in the removal of all strips not crossed by particles. Data are then stored in a temporary buffer to be sent via an ISA interface to a storage and data handling computer, a PC-104 board based on an AMD586 100 Mhz. A quartz clock is used to save event time; the beginning time of each session is noted to synchronize (in the off-line stage) the station time with the event time. Permanent data storage is performed on PCMCIA cards, periodically substituted and sent to Earth after each measurement sequence. For the Marco Polo Mission 4 660 Mbyte cards were used.

A typical session begins with the calibration of the silicon strips of the detector. This consists in the acquisition of 1024 pedestal events and the calculation of the pedestal average P_i and rms σ_i for each strip i. Thresholds T_i are set according to the formula $T_i = P_i + n\sigma_i$, with $n = 1$. The raw event, consisting in a 512 byte (256 channels * 2 byte/channel) matrix, is reduced by pedestal suppression with the removal of all hits below the threshold T_i. The choice of n was done compromising between data compression and strip hit lost to pedestal fluctuation due to temperature effects. Temperature drift, non negligible before thermal equilibrium in the device is reached (several hours after turn on), influences pedestal position; to compensate for this effect calibrations are repeated every 120 seconds. In Figure 6(top) is shown the position of the mean value of the pedestal of two sample strips as a function of time. If this is compared with temperature measurements (Figure 6-bottom) it is possible to see the correlation between the two behaviors, due to temperature dependent variations of the CR1 and electronics chain and to estimate temperature drift coefficient (Figure 7). In our case we obtain a value of 22.5 $ADC\ ch./^oC$. This effect does not affect detector noise: the histogram of the rms of the 256 detector strip at the beginning and at the end of the mission (Figure 8) shows that average pedestal rms is below 7 channels for the whole duration of the acquisition (one strip - not shown in the Figure - has a rms of 2000). Each calibration takes 2 seconds , after which particle acquisition begins. Each event also includes

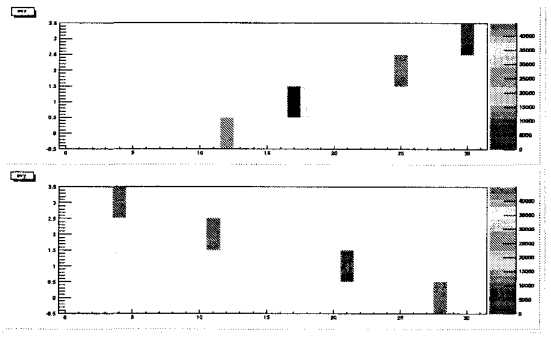

Figure 9. A Ne event crossing Sileye-3: Top Panel: X view, Bottom Panel Y, view; X axis: strip number, Y axis plane number.

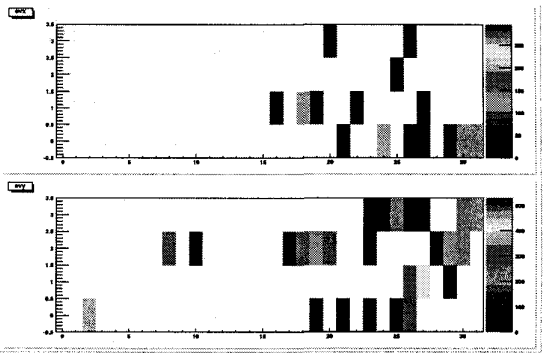

Figure 10. A showering event crossing Sileye-3: Top Panel: X view, Bottom Panel Y, view; X axis: strip number, Y axis plane number.

scintillator counters (S1, S2 , S1*S2) and clock, to synchronize it with the PC-104 clock. All events are stored in one of the two DSP buffers (15 kbyte each); when one of the buffer is filled the PC-104 begins data transfer while the second buffer is being filled. This procedure allows reduction of the dead time due to data transfer between the two CPU. The device has been tested on accelerator in Uppsala (TSL laboratory) with low energy ($\simeq 45 MeV/n$ D, C, O) and Dubna (500 MeV/n He).

3. SOYUZ-34 MISSION: FIRST RESULTS

Sileye-3 was placed on board of the International Space Station on April the 27th 2002 during the Soyuz-34 taxi flight mission. The cosmic ray detector was placed in the PIRS module (Figure 5) and was active for the whole duration of the mission, which lasted until May the 5th. 6 Light Flash and EEG sessions were performed by the Italian cosmonaut Roberto Vittori - part of the Soyuz-34 crew - resulting in the first controlled observation of Light Flashes on board the International Space Station. The PCMCIA cards with data were returned on ground with the Soyuz at the end of the mission. The whole dataset amounts to 131 hours, covering 87 station revolutions from 27/4/2002 to 2/5/2002. A typical cosmic ray event, a Neon nucleus crossing the device, is shown in Figure 9. One of the characteristics of Sileye-3 is its independent channel readout which allows acquisition of multi-particle events due to showers initiated with the interaction of primary particles with the hull or the equipment of the ISS: Figure 10 shows a typical event with this topology. The acquisition particle rate as a function of time is shown in Figure 11. The highest groups of peaks are due to passage in the South Atlantic Anomaly (SAA), where particle rate increases more that one order of magnitude due to the presence of the trapped proton component. In Figure 12 is shown the acquisition rate over a shorter time period. Here it is possible to see how particle rate is higher at the poles and lower at the geomagnetic equator. The long-term modulation of the peak maximum is due to longitudinal effects related to the 11^o offset of the geomagnetic field.

The particle spectum observed with Sileye-3 are shown in Figure 13. It is possible to see the typical features of the cosmic ray flux in space: the particle spectrum is dominated by protons and helium nuclei (the leftmost peak in Figure 13). The peak - containing H and He nuclei - has been cut for clarity and has an height of $6 \cdot 10^4$ counts. For higher Z particles it is possible to see how even-numbered nuclei are more abundant

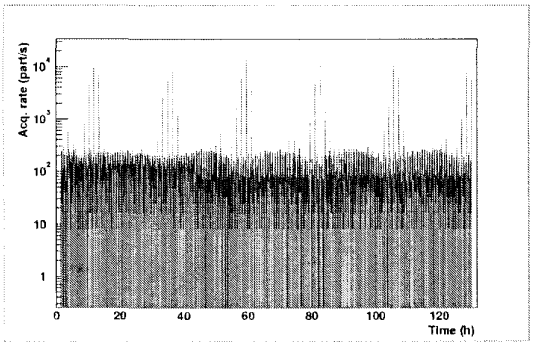

Figure 11. Cosmic ray flux vs time during the Soyuz-34 mission. Black: all particle rate; Grey: $Z > 5$ nuclei

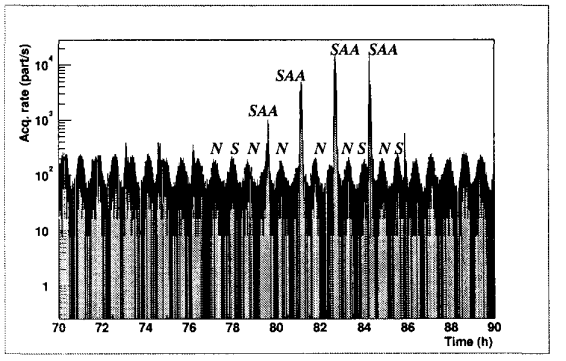

Figure 12. Cosmic ray flux vs time during the Soyuz-34 mission; note the passage in the SAA (higher peaks) and the modulation due to passage through the equator and the poles. Black: all particle rate; Grey: $Z > 5$ nuclei

than odd-numbered ones. The plot refers to high kinetic energy ($E > 100MeV/n$) particles, obtained requiring that the energy released in each plane do not differ by more than 20%. This value has been selected in order to allow for Landau fluctuations in the energy released in the silicon planes. Angle incidence correction has not been performed in this preliminary analysis, and therefore the peaks result widened due to the different angles of incidence in respect to the normal to the plane, resulting in variable path lengths inside the silicon wafers. The position of the peaks is increased by $1/cos(\theta_{ave})$, where θ_{ave} is the average angle of incidence of the detector on cosmic rays, equal for all nuclear species. This multiplicative factor does not affect the study of the detector linearity: at the energies considered particle energy loss in Silicon depends mostly from the square of the charge, so plotting the position of the nuclear peaks as a function of Z^2 it is possible to estimate the response of the device and its linearity, as shown in Figure 14. The good instrument response will allow to perform orbit dependent nuclear abundance studies to complement those done on the MIR with Sileye-2[28]. In addition, these data will be used to estimate absorbed dose and equivalent dose by the astronauts inside the ISS.

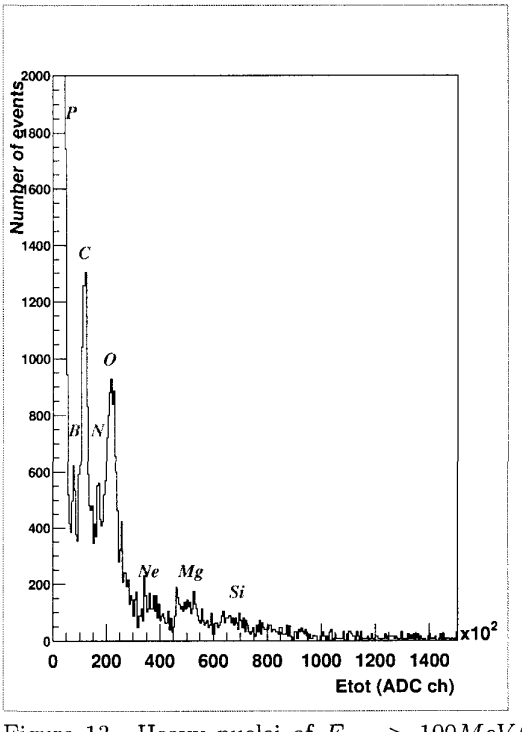

Figure 13. Heavy nuclei of $E_{kin} > 100MeV/n$ particles measured inside ISS. The proton peak (on the left) is cut for clarity and amounts to $2 \cdot 10^4$ counts.

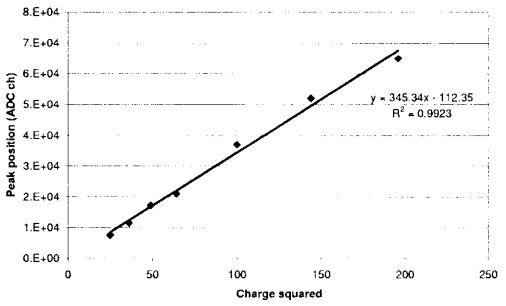

Figure 14. Peak position (ADC) vs square of the nuclear charge. The linear fit shows the good performance of the detector.

4. Conclusions

In this work we have presented the characteristics and the first results obtained with the Sileye-3/Alteino experiment on board the International Space Station. The performance of the detectors has been according to expectations; Light Flashes have been observed on board the International Space Station. Data analysis is currently in progress. The device will turned on again in the near future. A larger area detector, the Altea (Sileye-4) facility[31] is planned to be sent on the ISS by the end of 2003 to investigate the LF phenomenon and the study of cosmic ray radiation in space.

5. Acnowledgments

We thank all the staff of the TSL laboratory in Uppsala for their kind assistance during beam tests.

REFERENCES

1. Casolino M., Frascati Physics Series, XXIV, 195 (2001)
2. Reitz, G., et al., Rad. Meas, 26, 679 (1996)
3. Sakaguchi T., et al, NIM A 437, 75 (1999)
4. Badhwar, G., et al, IEEE Trans. on Nuc. Science 44(6), 2529 (1997)
5. Badhwar, G., Cucinotta, F. A., Rad. Res. 149, 209 1998.
6. Yasuda, H., et. al, Rad. Res. 154, 705 (2000)
7. Beaujan, R., et al, Rad Prot Dosim 85(1-4), 223 (1999)
8. Badhwar, G., Phys. Medica, XVII, Supp. 1 (2001)
9. Reitz, G., Phys. Medica XVII, Supp. 1. (2001)
10. Tobias, C. A., J. Aviat. Med., 23, 345 (1952)
11. Pinsky, L. S., Osborne, R. E, Bailey, J. V., Benson, R. E., Thompson, L. F., Science, 183, 957 (1974)
12. Osborne W. Z., Pinsky L. S., Bailey, J. V., NASA SP-368, 355 (1975)
13. Hoffman R. A., Pinsky L. A., Osborne W. Z., Bailey J. Z., NASA SP-377, 133 (1977)
14. Budinger, T. F., et. al, NASA TM X-58173, 13-1 (1976)
15. Budinger, T. F., et. al, NASA SP-412, 193 (1977)
16. Charman W. N., Dennis J. A., Fazio G. G., Jelley J. V., Nature 230, 522 (1971)
17. Tobias C. A., Budinger T. F., Lyman J. T., Nature 230, 596 (1971)
18. D'Arcy F. J., Porter N. A., Nature 196, 1013 (1962)
19. Charman, W. N., Rowlands, C. M., Nature, 232, 574 (1972)
20. McNulty P. J., Nature 234, 110 (1971)
21. McNulty P. J., Pease V. P., Bond V. P., Science 189, 453 (1975)
22. Horneck G., Nuc Tracks Radiat. Meas, **20 1**, 185 (1992)
23. Fazio G. G., Jelley J. V., Charman W. N., Nature 228, 260 (1970)
24. McNulty P. J., Pease V.P., Bond V. P., Science 201, 342 (1978)
25. Budinger T. F., Lyman J. T., Tobias C. A., Nature 239, 209 (1972)
26. Avdeev S., et al, Acta Astronautica, 50, 8, 511 (2002)
27. Bidoli V., et. al, NIM A, 424, 414 (1999)
28. Bidoli V., et. al, J. Phys. G, 27, 2051 (2001)
29. Adriani O., et. al, NIM A 478, 114 (2002)
30. Bonvicini V., et. al, NIM A 461, 262 (2001)
31. V. Bidoli, et. al, ESA SP-433, 505 (1999)